Atmospheric Environment 375 (2026) 122014

Contents lists available at ScienceDirect

Atmospheric Environment

journal homepage: www.elsevier.com/locate/atmosenv

Radon emissions from spring outlets: multi-scale assessment of local hotspots and regional atmospheric relevance

Sumeya B. Abdella [a], Michael T. Solomon [a], Luca Stabile [a,*], Michele Saroli [a], Giorgio Buonanno [a,b]

[a] Department of Civil and Mechanical Engineering, University of Cassino and Southern Lazio, Cassino, FR, Italy
[b] International Laboratory for Air Quality and Health, Queensland University of Technology, Brisbane, Qld, Australia

HIGHLIGHTS

- Direct quantification of radon flux from spring outlets.
- Multi-scale integration of flux and year-long monitoring.
- Springs create hotspots but negligible urban impact.
- Boundary-layer dynamics dominate outdoor radon variability.

ARTICLE INFO

Keywords:
Radon
Outdoor air quality
Spring water
Seasonal variation
Radon emission
Radon degassing

ABSTRACT

Radon (^{222}Rn) is a radioactive gas produced from the natural decay of uranium in soil, rock, and water, posing a significant health risk due to its association with lung cancer. While indoor radon has been extensively studied, radon degassing from groundwater sources and its contribution to outdoor air quality remain poorly characterized. This study quantifies radon emissions from spring outlets in the Cassino area (central Italy), integrating chamber-based emission measurements with year-long atmospheric monitoring. Emission rates per unit area reached up to 0.072 Bq m^{-2} s^{-1}, and atmospheric radon concentrations measured directly above spring outlets were up to 17 times higher than concurrent background levels, with peak values reaching 287 Bq m^{-3}. Continuous background monitoring revealed persistent diurnal variability driven by boundary-layer dynamics, with morning concentrations averaging 2.3 times the afternoon minimum and a clear seasonal maximum in autumn. Despite the pronounced localized enhancement, order-of-magnitude dilution estimates indicate that the contribution of individual spring outlets to the valley-scale atmospheric radon background is negligible. These results demonstrate that groundwater-fed springs can generate outdoor radon hotspots while exerting minimal influence on regional atmospheric concentrations, clarifying their role within the broader radon budget of carbonate aquifer systems influenced by major fault structures.

1. Introduction

1.1. Background

Radon is a radioactive, colorless, and inert noble gas that results from the natural decay of uranium found in rocks, soil, and water (Baltrėnas et al., 2020; Manawi et al., 2024). Because it is both colorless and inert, radon can move freely through permeable materials and enter the atmosphere or indoor environments through cracks and openings (Walczak et al., 2016). Globally, radon poses a significant environmental health risk, as it is strongly associated with lung cancer and is considered the second leading cause of the disease after cigarette smoking (Garzillo et al., 2017; Gaskin et al., 2018; Vienneau et al., 2021). Although a substantial body of research has focused on indoor radon levels and their health implications, its behaviors and transport in outdoor environments are comparatively less studied (Al-Zoughool and Krewski, 2009; Yarmoshenko et al., 2021). Outdoor radon concentrations tend to be lower due to dilution and atmospheric dispersion. Global

* Corresponding author.
E-mail address: l.stabile@unicas.it (L. Stabile).

https://doi.org/10.1016/j.atmosenv.2026.122014
Received 4 March 2026; Received in revised form 30 March 2026; Accepted 7 April 2026
Available online 7 April 2026

average outdoor radon concentrations range from 5 to 15 Bq m^{-3} (0.135-0.405 pCi L^{-1}), with the United States reporting an average of approximately 15 Bq m^{-3} (0.4 pCi L^{-1}), compared to indoor averages of 48 Bq m^{-3} (1.3 pCi L^{-1}) ((EPA), 2016). While regulatory limits exist for indoor radon, such as the U.S. EPA's 150 Bq m^{-3} (4 pCi L^{-1}) and WHO's 100 Bq m^{-3} (2.7 pCi L^{-1}), no specific guidelines have been established for outdoor environments ((EPA), 2016; Zeeb et al., 2009). Nevertheless, outdoor radon concentrations can vary significantly depending on geological, meteorological, and atmospheric conditions (Čeliković et al., 2022). These fluctuations are particularly noteworthy in regions with uranium-rich substrates, such as volcanic or sedimentary formations, where radon may escape from the ground into the air, potentially leading to localized exposure risks (Al-Zoughool and Krewski, 2009). In response to the spatial heterogeneity associated with geological controls, systematic radon monitoring initiatives have been strengthened in several countries. In Italy, for example, important developments include the creation of two monitoring networks for radon in air (Piersanti et al., 2025) and in water (Tallini et al., 2025).

1.2. Relevance of radon as an indicator of indoor and outdoor air quality

Radon is a crucial indicator of air quality, particularly for radiological health risks. This radioactive gas is produced by the natural decay of uranium present in soil and rocks, thereby contributing to exposure to ionizing radiation (Darby et al., 2005; Zeeb et al., 2009). Elevated radon levels indoors are especially concerning since people spend a significant amount of time in indoor spaces, where radon can accumulate in poorly ventilated areas, such as homes and office buildings (Rathebe et al., 2025). Radon can also reach the atmosphere from groundwater, natural gas, oceans, and human activities (Čeliković et al., 2022). While outdoor radon levels are usually lower, they help establish a baseline for natural background radiation and identify areas with high geological radon potential. Monitoring outdoor radon is essential for understanding regional variations, which can inform zoning regulations and building codes. Therefore, the presence and concentration of radon both indoors and outdoors offer valuable insights into air quality in both natural and constructed environments, informing environmental risk assessments and public health strategies ((EPA), 2016; (AuthorAnonymous, 2000)).

1.3. Importance of studying radon emissions from groundwater

Naturally occurring radioactive elements, such as radon, originate in rocks and soil and can dissolve into surface and groundwater (Dołhańczuk-Śródka et al., 2025; Nayak et al., 2022). Radionuclides, including ^{40}K, ^{226}Ra, ^{232}Th, ^{238}U, and ^{222}Rn, have been detected at trace levels in water sources worldwide (Choudhury et al., 2022; Sulaiman et al., 2025). The presence of these substances can pose health risks through radiation exposure from ingested radon, inhalation of radon released from water, and dermal absorption during activities such as bathing (Florou et al., 2006; Pyuskyulyan et al., 2024). Therefore, continuous monitoring and regulation of natural radioactivity levels in water is essential to safeguard public health.

When radon gas is emitted from groundwater sources, it can accumulate in nearby outdoor and indoor spaces, particularly in poorly ventilated environments, posing long-term exposure risks and increasing the likelihood of lung cancer (Darby et al., 2005; Zeeb et al., 2009). Although radon degassing from groundwater has been widely investigated in hydrogeological contexts, most studies have focused on using ^{222}Rn as a tracer of groundwater-surface water interactions rather than quantifying its atmospheric emission flux under open-air conditions. Direct measurements of radon emission rates from discrete spring outlets are scarce (Horváth et al., 2000; Sola et al., 2012), and only a limited number of studies have quantified near-field atmospheric enhancements (e.g., concentration transects from spring outlets) rather than evaluating outlet emissions against a concurrently monitored atmospheric background over extended periods (Guida et al., 2014). Furthermore, the integration of point-source degassing measurements with long-term atmospheric radon monitoring remains largely unexplored, particularly in carbonate aquifer systems influenced by major fault structures. As a result, the relative importance of groundwater-fed springs as localized outdoor radon hotspots compared to diffuse soil exhalation is still poorly constrained.

1.4. Aims of the work

This study addresses these gaps by providing a field-based framework to quantify groundwater-derived radon emissions in open-air spring systems, using Cassino as a representative carbonate aquifer system influenced by major fault structures. Indeed, Cassino, Central Italy, represents a region with volcanically influenced and tectonically active geology that controls groundwater radon levels, as documented in central Italian aquifers and spring waters (Piersanti et al., 2025; Tallini et al., 2025). This study advances current understanding in three key ways. First, it provides direct chamber-based quantification of radon emission fluxes from discrete groundwater-fed spring outlets under open-air conditions. Second, it integrates these microscale flux measurements with year-long atmospheric radon monitoring, enabling a multi-scale assessment of localized enhancements relative to regional background variability. Third, it evaluates the relative source strength of spring degassing compared to diffuse soil exhalation, thereby clarifying the actual contribution of groundwater outlets to urban-scale atmospheric radon levels. This approach enables a quantitative multi-scale assessment of radon emissions, from localized degassing at spring outlets to valley-scale atmospheric dynamics.

2. Methodology

2.1. Study area

The study was conducted in Cassino (Lazio, central Italy), located in the Latina Valley at the foothills of Monte Cassino and Monte Cairo (Fig. 1). The area is characterized by sedimentary formations (calcareous, clayey-arenaceous, and fluvial-lacustrine) with heterogeneous permeability, influenced by deep fault systems that facilitate the upward migration of radon from the crust to the surface. The study area represents a carbonate aquifer system in which groundwater circulation and spring emergence are strongly influenced by major fault structures. Radon accumulates within the extensive carbonate aquifers associated with the hydrostructures of the study area (Saroli et al., 2014, 2020). As a radioactive noble gas produced by uranium decay, radon behaves as a geochemical tracer, migrating preferentially through high-permeability zones generated by fault-related fracture networks within the reservoir rocks. It can also be transported along fault zones by carrier gases such as CO_2 and CH_4 (Etiope and Martinelli, 2002).

The investigation focused on three spring sources that are part of a hydrographic network originating from Monte Cassino and ultimately discharging into the Gari River. The Cassino plain hosts an unconfined carbonate aquifer associated with the Monte Cairo-Monte Cassino hydrostructure, as well as a multilayered aquifer system developed within Quaternary fluvial-lacustrine deposits. Groundwater flow feeding the Gari springs is strongly controlled by major fault systems, including regionally significant structures with documented Quaternary activity, which enhance subsurface circulation and may facilitate radon transport (Saroli et al., 2019, 2020). Three sampling sites were selected along the Gari spring system in Cassino (Fig. 1). These sites were selected based on their varying outlet sizes, water discharge, and turbulence characteristics to enable comparison of radon emissions under different hydrogeological and hydrological conditions. Site 1 (Gari spring, i.e., “Sorgente del Gari”) is located behind Piazza Corte, where groundwater emerges through fractured carbonate rocks under relatively low-flow conditions and represents the primary source of the Gari River. Site 2 (Municipal Park of Cassino, known as “Parco XV Marzo,

Fig. 1. Geographic framework of the study area: location of Cassino (central Italy) and detailed view of the Monte Cassino area showing the three sampling sites (springs) and the background site.

1944") extends along a widened section of the Gari River within the urban park area; this site corresponds to the largest outlet, characterized by higher water discharge and localized turbulence associated with channel morphology and hydraulic structures. Site 3 (Horti di Porta Paldi, a public park known as "Parco del Gari") is a historic green area located downstream within the broader Parco del Gari. All three selected sites feed into the Gari River, with Site 1 representing its primary source.

2.2. Measurement of radon concentration at the sampling sites

Radon levels were measured using the Aranet Radon Plus (Rn+) sensors, wireless devices capable of detecting radon concentrations from 0 to 7900 Bq m^{-3}. The sensors employ ionization chamber technology, enabling precise, real-time radon monitoring. In addition to radon, the sensors simultaneously recorded temperature (0-50 °C, ±0.3 °C accuracy) and relative humidity (0-85%, ±3% accuracy), providing comprehensive environmental monitoring. The sensors recorded measurements at 10-min intervals and were calibrated according to the manufacturer's specifications before deployment.

Two complementary monitoring approaches were employed. For continuous background monitoring, one sensor was installed on the second-floor balcony of the Department of Civil and Mechanical Engineering at the University of Cassino and Southern Lazio, in an open, well-ventilated area approximately 180 m from the nearest spring source. This sensor operated continuously from January 2025 to January 2026, recording atmospheric radon levels under natural environmental conditions and providing baseline data for comparison.

For site-specific measurements, a sensor was deployed at each of the three spring sites. At each location, the sensor was suspended near the spring outlet approximately 5-10 cm above the water surface to capture radon immediately released from the water (Fig. 2). Placement on adjacent dry land was avoided, as this would have increased the distance

Fig. 2. Details of the positioning of the sensor for in situ measurements at the three different springs.

from the emission source and reduced sensitivity to localized degassing. The sensor was secured using existing protective railings or fixed structures at each site, allowing stable suspension above the water without direct contact. Measurements were conducted for several hours over multiple days to capture spatial variability, spanning May and July 2025.

2.3. Evaluation of the radon emission rates per unit area

To quantify radon emission rates per unit area of the spring sources, a chamber-based accumulation method was employed at Sites 1 and 2. A plastic storage box with a volume of 0.21 m^3 (80 × 60 × 43 cm), open at the bottom, served as the accumulation chamber. Five small holes were drilled in the top of the chamber, four at the corners and one at the center. Ropes were threaded through the four corner holes to suspend the entire chamber approximately 5 cm above the water surface with the open side facing downward, while a rope through the central hole suspended the radon sensor inside the chamber (Fig. 3). The configuration prevented direct water contact while capturing radon degassing from the water surface. Measurements were conducted during June to July 2025 (representing summer conditions) and December 2025 to January 2026 (representing winter conditions). This seasonal approach enabled assessment of temporal variability in radon emissions and concentrations between warm and cold periods. The Aranet Radon Plus sensor was suspended inside the chamber at mid-height to monitor radon accumulation over time. Measurements were conducted over 2-4-h periods during which radon concentrations increased from background levels to equilibrium. Each site was measured on multiple occasions (3-5 times) across different seasons to assess temporal variability in emission rates. Background measurements were used to establish baseline concentrations for emission rate calculations. The radon emission rate per unit area of the spring (E, Bq m^2 s^{-1}) was calculated using the mass balance equation:

$$E = \frac{(C_t - C_{back})\cdot V}{A\cdot t} \quad \left(Bq\ m^{-2}\ s^{-1}\right) \qquad \text{eq. 1}$$

where C_t is the radon concentration inside the chamber at time t (Bq m^{-3}), C_{back} is the background radon concentration measured at reference location (Bq m^{-3}), V is the chamber volume (0.21 m^3), A is the chamber base area in contact with emission source (0.48 m^2), and t (s) represents the time duration of radon accumulation. The emission rate per unit area of the spring was calculated from the linear portion of the radon accumulation curve, typically observed during the first 2-4 h of chamber deployment, before equilibrium conditions were reached.

2.4. Statistical analysis

Statistical analyses were performed using Python (version 3.12). Due to the non-normal distribution of radon concentration data (confirmed by Shapiro-Wilk test, $p < 0.05$), non-parametric tests were employed, following established protocols for environmental radon studies (Iwata et al., 2018; Pignatelli et al., 2025). Wilcoxon rank-sum tests (also known as Mann-Whitney U tests) were used to compare radon concentrations at each site with its background level, consistent with methodologies applied in previous radon monitoring studies (Fagerland and Sandvik, 2009). Kruskal-Wallis tests followed by Dunn's post-hoc pairwise comparisons with Bonferroni correction were used to compare radon concentrations among the three sites, an approach widely adopted in environmental radon research for multi-group comparisons (Bewick et al., 2004). Statistical significance was set at $\alpha = 0.05$.

To evaluate the association between atmospheric radon concentrations and meteorological parameters (temperature, relative humidity, and atmospheric pressure), non-parametric Spearman rank correlation coefficients (ρ) were calculated using hourly averaged data from the background monitoring station. Spearman correlation was selected due to the non-normal distribution of radon concentrations and the potential presence of non-linear relationships between variables. Statistical significance was assessed at $\alpha = 0.05$. For descriptive purposes, the squared correlation coefficient (ρ^2) was used as an approximate indicator of each variable's relative explanatory power, providing a first-order estimate of the proportion of variance associated with the observed relationships.

Moreover, the association between background radon concentrations and airborne particle concentrations in Cassino was also investigated. In particular, correlations were performed with daily average particle number and PM_{10} concentrations. Particle number concentration data were obtained during an experimental campaign conducted alongside radon measurements at the background site mentioned above. The measurements were carried out using a diffusion charger, the Partector Pro 2 (Naneos particle solutions gmbh), which can measure total particle number concentrations and size distributions of ultrafine

Fig. 3. Experimental apparatus deployed to evaluate the radon emission rate of the unit area of the two springs (Sites 1 and 2).

particles in the range 10-300 nm with a sampling frequency of 6 s. PM_{10} concentrations were retrieved from the fixed sampling point placed in Cassino by the regional Environmental Protection Agency (ARPA Lazio). Correlations were assessed using a non-parametric Spearman rank correlation coefficient calculated from daily-averaged data. In this case, ρ^2 was similarly used to compare the relative strength of the particle number- and PM_{10}-radon relationships with that observed for individual meteorological parameters.

3. Results and discussion

3.1. Radon concentrations at monitored sites

In Fig. 4, illustrative examples of radon concentration trends measured at the three sites, along with the simultaneous background values, are reported to clearly illustrate the distinct behavior observed at each site. A marked contrast emerges among the three locations. Site 2 exhibits a strong and highly elevated radon signal, consistently well above background levels, indicating intense groundwater degassing. Site 1 shows more moderate concentrations with fluctuations that are comparable to background variability, suggesting a weaker or more diffuse emission. In contrast, Site 3 is characterized by relatively stable radon concentrations that remain consistently above background, indicating persistent but less dynamic degassing conditions. These observations provide a qualitative framework for interpreting the statistical differences among sites, which are quantified in Fig. 5.

In Fig. 5, the radon concentration statistics measured at three sites, along with the simultaneous background levels, are presented as box plots. At Site 1, during the monitoring period, the median radon concentration was 35 Bq m^{-3} (interquartile range: 26-53 Bq m^{-3}), significantly higher than the concurrent background value of 18 Bq m^{-3} (interquartile range: 13-25 Bq m^{-3}; $p = 0.001$). However, concentrations at this site remained lower than those observed at the other locations. Site 2 exhibited the highest radon levels, with a median concentration of 287 Bq m^{-3} (interquartile range: 157-393 Bq m^{-3}) compared with a background median of 17 Bq m^{-3} (interquartile range: 14-26 Bq m^{-3}). Concentrations at Site 2 were significantly higher than both background ($p < 0.0001$) and Site 1 ($p = 0.0113$), as determined by Kruskal–Wallis and post hoc pairwise comparisons. Site 3 showed intermediate values, with a median radon concentration of 48 Bq m^{-3} (interquartile range: 45-53 Bq m^{-3}), significantly higher than the simultaneous background (median 17 Bq m^{-3}; $p = 0.015$) but significantly lower than Site 2 ($p = 0.0092$). Overall, radon concentrations increased progressively from Site 1 to Site 3 to Site 2. On the contrary, baseline atmospheric radon levels were consistent across measurement periods (17-18 Bq m^{-3}) and did not differ significantly ($p = 0.977$), confirming that spatial differences observed near the spring outlets were attributable to local groundwater emissions rather than temporal variability in background conditions. These results confirm the distinct signal characteristics observed in Fig. 4.

The observed spatial variability is consistent with the physical mechanisms governing radon transfer across the water-air interface. Radon degassing is controlled by a transfer velocity coefficient that increases with turbulence and water discharge. Under low-turbulence conditions, transfer velocities are relatively small (on the order of 10^{-6} m s^{-1}), resulting in slower radon escape from water to air (Ongori et al., 2015). Accordingly, the relatively stable hydrodynamic conditions at Site 1 likely limited radon degassing despite elevated groundwater concentrations.

More generally, radon concentrations in surface waters are regulated by radioactive equilibrium, recoil diffusion, and losses through degassing at the water-air interface (Adyasari et al., 2023; Ellins et al., 1990; Hoehn and Von Gunten, 1989). Efficient degassing is promoted by increased turbulence and temperature (Adyasari et al., 2023). The substantially higher concentrations observed at Site 2, approximately 17 times background, compared with a twofold increase at Site 1, are therefore consistent with its larger outlet size and higher discharge, which enhance mixing and radon transfer to the atmosphere (Cartwright and Hofmann, 2016; Cook, 2013; Mullinger et al., 2007). Together, these results indicate that hydrological characteristics, particularly outlet size, discharge, and turbulence, play a primary role in modulating radon release efficiency in groundwater-fed spring systems. These measurements confirm that spring outlets can act as localized outdoor radon hotspots under open-air conditions.

3.2. Temporal patterns in background radon concentrations

To complement the site-specific measurements, continuous background radon monitoring was conducted over one year (January 2025-January 2026) to characterize seasonal and diurnal variations in atmospheric radon levels. Understanding these temporal patterns is essential for interpreting the contribution of groundwater sources to

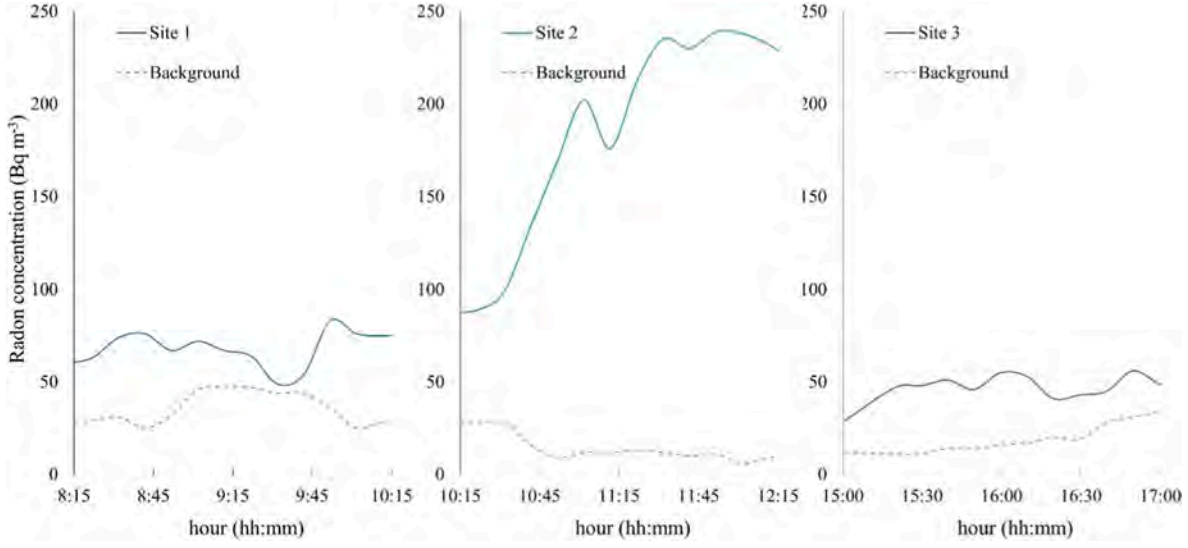

Fig. 4. Illustrative example of radon concentration trends measured at the three spring sites (Site 1, Site 2, and Site 3) during the monitoring campaigns. The dashed line represents the corresponding background radon concentration measured at the reference station. All panels share the same y-axis scale to facilitate direct comparison among sites.

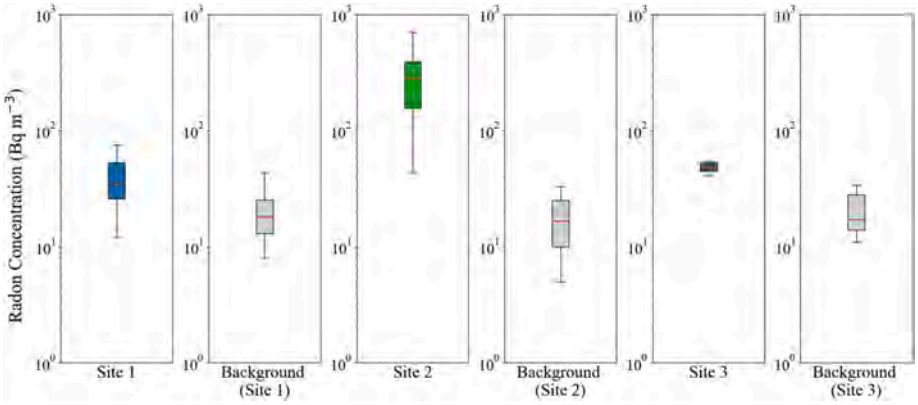

Fig. 5. Boxplots of radon concentrations measured at the three spring sites (Site 1, Site 2, and Site 3) and corresponding simultaneous background levels. The central red line represents the median; the box indicates the interquartile range (IQR); and whiskers extend to the 5th and 95th percentiles, excluding outliers. (For interpretation of the references to color in this figure legend, the reader is referred to the Web version of this article.)

local radon concentrations and for assessing exposure risks in valley environments like Cassino. The monitoring data revealed pronounced diurnal patterns, with radon concentrations consistently higher at night than during the day (Fig. 6). The dynamics of the atmospheric boundary layer drive this pattern. During colder periods and at night, the atmospheric mixing layer descends closer to the surface, reducing vertical dispersion and enhancing the accumulation of ground-level pollutants, including radon (Chambers et al., 2011; Zahorowski et al., 2004). Conversely, daytime warming elevates the mixing layer, promoting dilution and dispersion.

Radon concentrations typically increased overnight, peaking around 6:00 a.m. After this peak, concentrations declined as outdoor temperatures rose and the atmospheric mixing layer elevated, promoting dispersion. Morning peak concentrations were on average 2.3 times higher than afternoon minimum concentrations (14:00-17:00) (Fig. 6), a difference that was highly significant across all seasons (Wilcoxon signed-rank test, $p < 0.001$). This pattern aligns with previous studies on outdoor radon behavior, which have consistently found that radon levels peak in the mornings, with concentrations remaining lower in the afternoon (Kolarž et al., 2009; Schubert et al., 2018). The consistency of this diurnal pattern across all seasons underscores the dominant influence of atmospheric dynamics on radon dispersion in outdoor environments, even relative to the variability of the emission factor.

In addition to diurnal variations, year-round background monitoring data revealed significant seasonal fluctuations in atmospheric radon concentrations. Fig. 7 illustrates the daily atmospheric radon concentrations measured at the background station over the one-year monitoring period. The dataset exhibits evident diurnal and seasonal variability, with intermittent peak events. The mean radon concentration at the background monitoring station was highest during the autumn (Fig. 7), while the lowest mean concentrations were recorded during the spring. This seasonal pattern, with an autumn peak in outdoor atmospheric radon, has been consistently documented in long-term outdoor monitoring studies and differs from the typical winter-maximum pattern observed in indoor environments, which is due to the reduced ventilation of the buildings during the colder season (A. Podstawczyńska et al., 2010; Bossew and Lettner, 2007; Caracci et al., 2024, 2022, 2021).

The autumn peak observed at the background station likely reflects the combined influence of atmospheric and soil processes. During autumn, the progressive reduction in mixing layer height limits vertical dispersion, while moderate surface temperatures prevent strong convective dilution (Hayashi et al., 2015). In parallel, increased soil moisture enhances radon partitioning from pore water into soil gas, potentially increasing soil radon concentrations by 10-20% compared to drier conditions (Arvela et al., 2015). These interacting factors create favorable conditions for radon accumulation in near-surface air.

The seasonal amplitude recorded at the background station underscores the importance of year-round monitoring when characterizing baseline outdoor radon levels in geologically complex environments.

To provide a concise quantitative summary of seasonal variability, the main statistical descriptors of atmospheric radon concentration and meteorological parameters are reported in Table 1. Median radon concentrations exhibit a clear seasonal pattern, with the highest values observed in autumn and the lowest in spring, while winter and summer display intermediate values. The percentile ranges further highlight

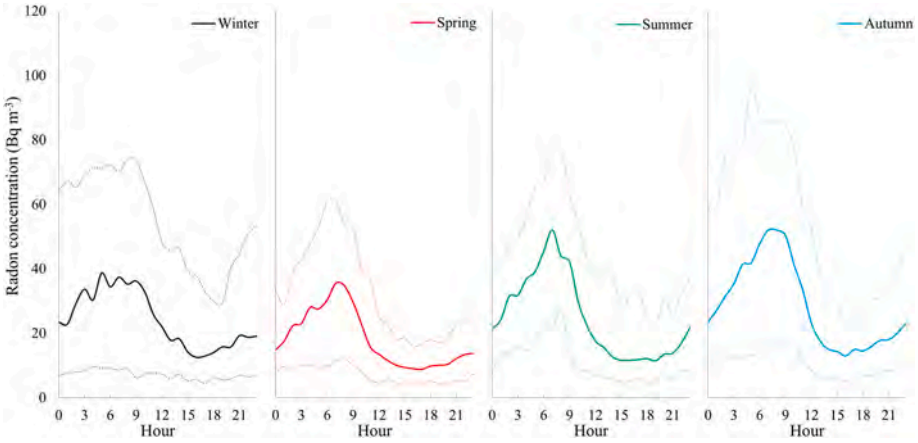

Fig. 6. Median hourly radon concentrations measured at the background monitoring station during different seasons, dashed lines represent 5th and 95th values.

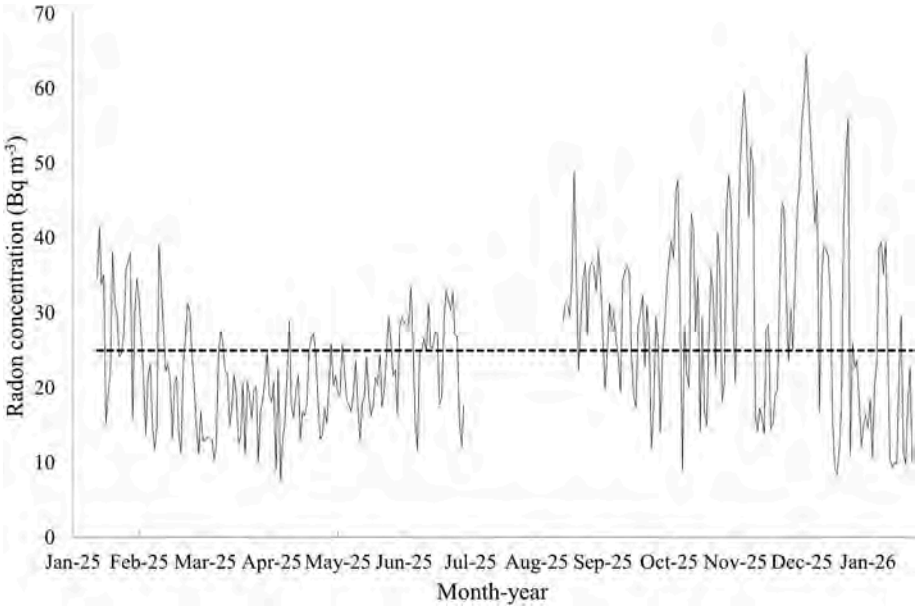

Fig. 7. Daily outdoor radon concentrations measured at the background monitoring station from January 2025 to January 2026. The dashed line represents the annual median concentration (24 Bq m^{-3}).

Table 1
Seasonal statistics of atmospheric radon concentration and meteorological parameters measured at the background site. Values are reported as median (5th-95th percentile range).

	Radon concentration (Bq m^{-3})	Temperature (°C)	Relative humidity (%)
Winter	21.2 (6.7-63.1)	12.2 (7.7-17.1)	68.8% (45.3-82.8%)
Spring	14.8 (5.3-44.7)	18.0 (11.8-26.6)	59.0% (36.2-73.6%)
Summer	22.2 (6.8-59.3)	30.2 (23.9-39.6)	46.2% (28.9-60.9%)
Autumn	23.8 (8.0-71.1)	19.5 (11.3-30.5)	61.3% (34.0-79.5%)

substantial intra-seasonal variability, particularly during autumn and winter, suggesting more frequent accumulation events under stable atmospheric conditions. The seasonal variation in radon concentration is consistent with observed meteorological patterns: higher summer temperatures promote atmospheric mixing, while more stable conditions in autumn favor radon accumulation.

To further quantify the influence of meteorological conditions on the observed temporal variability, a correlation analysis was performed between radon concentrations and key atmospheric parameters. Spearman correlation analysis of the hourly-averaged background dataset ($n = 4480$) revealed statistically significant but moderate associations between atmospheric radon concentrations and meteorological parameters. Radon exhibited a weak negative correlation with air temperature ($\rho = -0.19$) and a weak positive correlation with relative humidity ($\rho = 0.14$), while a stronger positive correlation was observed with atmospheric pressure ($\rho = 0.35$) (all $p < 0.001$). In terms of explanatory power, individual meteorological parameters account for a limited fraction of total radon variability ($\rho^2 < 0.15$), indicating that no single variable exerts dominant control. The negative relationship with temperature is consistent with enhanced daytime atmospheric mixing, in which higher temperatures promote convective turbulence and a higher boundary-layer height, resulting in more efficient vertical dilution of radon. Conversely, lower temperatures, particularly during nighttime and colder periods, favor reduced mixing and radon accumulation near the surface. The positive association with atmospheric pressure likely reflects the stabilizing effect of high-pressure systems, which suppress vertical mixing and prolong radon's residence time in the near-surface layer. Overall, these results highlight that outdoor radon concentrations are governed by multi-factorial boundary-layer dynamics rather than isolated meteorological drivers, despite the statistical robustness of the observed correlations.

To further test the role of atmospheric stability, the correlation between radon and airborne particle concentrations was examined. Indeed, high airborne particle concentrations in the city of Cassino are recognized as due to thermal inversion and a reduced boundary layer (ARPA Lazio, 2009). The analysis revealed a moderate-to-strong, statistically significant, positive correlation between daily radon and PM_{10} concentrations ($\rho = 0.50$, $p < 0.001$) and radon and particle number concentrations ($\rho = 0.34$, $p < 0.001$) on the entire monitoring period. These correlations were stronger ($\rho = 0.79$, $p < 0.001$ for PM_{10} and $\rho = 0.63$, $p < 0.001$ for particle number) when the analysis was limited to the colder period (November to March), i.e., when the boundary layer is lower and thermal inversions are more frequent. These correlations serve as a surrogate to confirm the larger effect of the mixing layer on radon concentration relative to other meteorological parameters.

Individual meteorological parameters account for a limited fraction of total radon variability ($\rho^2 < 0.15$), whereas airborne particles, used here as a surrogate for boundary-layer stability, explain a substantially larger fraction of the variance (ρ^2 about 0.25 for the full dataset and up to 0.62 during colder months for PM_{10}). This confirms that atmospheric stability and mixing-layer dynamics represent the dominant controls on outdoor radon concentrations.

3.3. Radon emission rates per unit area and seasonal variability

To quantify the radon flux from groundwater sources, emission rates per unit area were evaluated at Sites 1 and 2 using the chamber accumulation method during both summer (May-July 2025) and winter (December 2025-January 2026) periods as described in section 2.3.

At Site 2, the calculated average radon emission rate per unit area of the spring was 0.072 Bq m^{-2} s^{-1} (with a standard deviation of 0.016 Bq m^{-2} s^{-1}) in summer and 0.045 Bq m^{-2} s^{-1} (with a standard deviation of 0.019 Bq m^{-2} s^{-1}) in winter, indicating that summer emissions were approximately 1.6 times higher than winter values. At Site 1, the average emission rate per unit area of the spring was 0.044 Bq m^{-2} s^{-1}

(with a standard deviation of 0.014 Bq m^{-2} s^{-1}) in summer and 0.055 Bq m^{-2} s^{-1} (with a standard deviation of 0.026 Bq m^{-2} s^{-1}) in winter. Seasonal differences in emission rates per unit area were assessed using a Mann–Whitney *U* test. Although median summer fluxes at Site 2 were approximately 1.6 times higher than winter values, the difference did not reach statistical significance. At Site 1, winter fluxes were slightly higher than summer values; however, no statistically significant seasonal difference was detected either. Overall, these results indicate that the observed seasonal contrasts should be interpreted cautiously, as intra-seasonal variability and limited sample size reduce statistical power and prevent firm conclusions regarding systematic seasonal effects. These contrasting seasonal patterns between the two sites reflect the interplay of multiple environmental factors controlling radon emissions from groundwater. In particular, the higher summer emissions observed at Site 2 are consistent with temperature-dependent degassing processes. Increased water temperatures reduce radon solubility and enhance its transfer from water to air, whereas lower winter temperatures favor radon retention in the aqueous phase (Hoehn and Von Gunten, 1989). This temperature effect is particularly pronounced at sites with high discharge and turbulence, where efficient water-air interface mixing facilitates rapid degassing.

To contextualize the measured emission rates per unit area, a comparison with reported radon fluxes from other natural surfaces is informative. The spring emission rates per unit area observed in this study (0.044-0.072 Bq m^{-2} s^{-1}) exceed the UNSCEAR estimate of mean worldwide soil radon exhalation (about 0.016 Bq m^{-2} s^{-1} (UNSCEAR, 2000),) and are comparable to or higher than the upper range reported for many soils, including fault-controlled settings. In contrast, atmospheric evasion fluxes estimated for lake surfaces are typically orders of magnitude lower (tens of Bq m^{-2} d^{-1}, i.e., about 10^{-4} Bq m^{-2} s^{-1} (Sun et al., 2025),), reflecting weaker turbulence and distributed exchange over larger water bodies. Fluxes measured in riverbed or sediment contexts are also generally lower (on the order of 10^{-3}-10^{-2} Bq m^{-2} s^{-1} (Koschorreck et al., 2022),). This comparison indicates that groundwater-fed spring outlets can act as localized, high-intensity degassing points, with emission rates per unit area comparable to or exceeding typical soil exhalation rates, despite their limited spatial extent.

Beyond process-based considerations, the magnitude of the measured fluxes also warrants evaluation in a regulatory context. From a regulatory perspective, European legislation establishes reference levels for indoor radon concentrations under Council Directive 2013/59/Euratom (European Commission, 2013), which was transposed into Italian law through Legislative Decree No. 101/2020 (Repubblica Italiana, 2020); however, these frameworks do not specify threshold values for environmental radon emission rates per unit area or outdoor atmospheric radon concentrations. Therefore, interpretation of the measured fluxes requires comparison with international technical standards. In China, the mandatory standard GB 50325-2020 for Indoor Environmental Pollution Control of Civil Building Engineering classifies construction sites according to soil radon exhalation rates. Specifically, radon exhalation rates below 0.02 Bq m^{-2} s^{-1} are classified as safe, values between 0.05 and 0.10 Bq m^{-2} s^{-1} as requiring preventive measures, and values above 0.30 Bq m^{-2} s^{-1} as necessitating mitigation (GB 50325, 2020). In comparison, the emission rates per unit area measured in this study remain below 0.10 Bq m^{-2} s^{-1}; however, summer emissions at Site 2 and winter emissions at Site 1 (0.08 Bq m^{-2} s^{-1}) approach the lower precautionary threshold. Although indoor exposure remains the primary radiological health concern, these findings suggest that environmental radon sources in groundwater-fed carbonate aquifer systems may warrant consideration in land-use planning and radon risk assessment in similar geological settings.

To further assess the potential relevance of spring outlets to the surrounding atmospheric background, we performed a rough comparison of the source strength of spring degassing with that of diffuse soil exhalation. The total emission from a spring outlet is the product between the radon emission rate per unit area of the spring (*E*, Bq m^2 s^{-1}) and the effective degassing area. Even considering the maximum value of radon average emission rate per unit area (i.e., 0.072 Bq m^{-2} s^{-1} for Site 2 in summer), the total emission rate (i.e., per unit time) would be in the range 0.1-3.6 Bq s^{-1} if a degassing area ranging between 2 and 50 m^2 is adopted.

For comparison, adopting the abovementioned UNSCEAR global mean soil radon exhalation rate (about 0.016 Bq m^{-2} s^{-1} (UNSCEAR, 2000),), just 1 km^2 of soil emitting area would result in a total emission rate of 16 000 Bq s^{-1}. Even substantially smaller emitting surfaces (e.g., a few hectares) would produce source strengths orders of magnitude greater than that of an individual spring outlet.

This comparison indicates that, although spring outlets can generate intense radon enhancements at the microscale immediately above the water surface, their integrated emissions are negligible relative to diffuse soil exhalation across the broader valley floor. Consequently, the elevated concentrations measured near the spring represent localized degassing hotspots rather than a dominant contributor to the city-scale atmospheric radon background. To assess whether a single spring outlet could meaningfully affect atmospheric radon at the urban scale, an order-of-magnitude steady-state dilution estimate can be easily performed: considering the total emission of the direct source evaluated above of 3.6 Bq s^{-1} and assuming representative winter daytime conditions with an effective mixing height of 100 m (Cassino may present such limited mixing height during cold periods), a dilution over a characteristic urban length scale of 100 m, and a mean wind speed of 1 m s^{-1}, this emission would be diluted within by an air flow rate of about 10 000 m^3 s^{-1}. Under these conditions, the expected concentration enhancement would be on the order of 3.6×10^{-4} Bq m^{-3}: this value is several orders of magnitude lower than the observed atmospheric background levels (tens of Bq m^{-3}), representing less than 0.002% of the typical background concentration. These findings indicate that individual spring outlets have limited regional atmospheric relevance despite their pronounced local intensity. These calculations quantitatively confirm that, although spring outlets generate intense microscale radon hotspots immediately above the water surface, their integrated contribution to valley-scale atmospheric radon remains negligible under realistic dispersion conditions. To provide a conceptual synthesis of the multi-scale processes investigated in this study, Fig. 8 illustrates the contrast between localized radon enhancements above spring outlets and their negligible contribution to valley-scale atmospheric background levels.

3.4. Study strengths and limitations

This study combines direct chamber-based quantification of radon emission rates per unit area with year-long atmospheric background monitoring, enabling a quantitative multi-scale assessment of groundwater-derived radon emissions. A major strength lies in integrating microscale measurements from discrete spring outlets with continuous background observations, enabling evaluation of both localized enhancements and regional-scale relevance. The use of nonparametric statistical methods, which are appropriate for skewed environmental datasets, further strengthens the robustness of the analysis. Moreover, the comparison between spring emission fluxes and diffuse soil exhalation provides a physically grounded framework for interpreting source strength within a broader atmospheric radon budget.

Nonetheless, several limitations should be acknowledged. First, site-specific measurements were limited to three spring outlets within a single fault-influenced carbonate hydrogeological setting. Although representative of similar carbonate systems, the findings may not be directly transferable to other geological contexts without additional validation. Second, emission rate measurements were conducted only during summer and winter campaigns; transitional seasons (spring and autumn) were not directly sampled for flux estimation, potentially limiting the characterization of intermediate hydrological and thermal

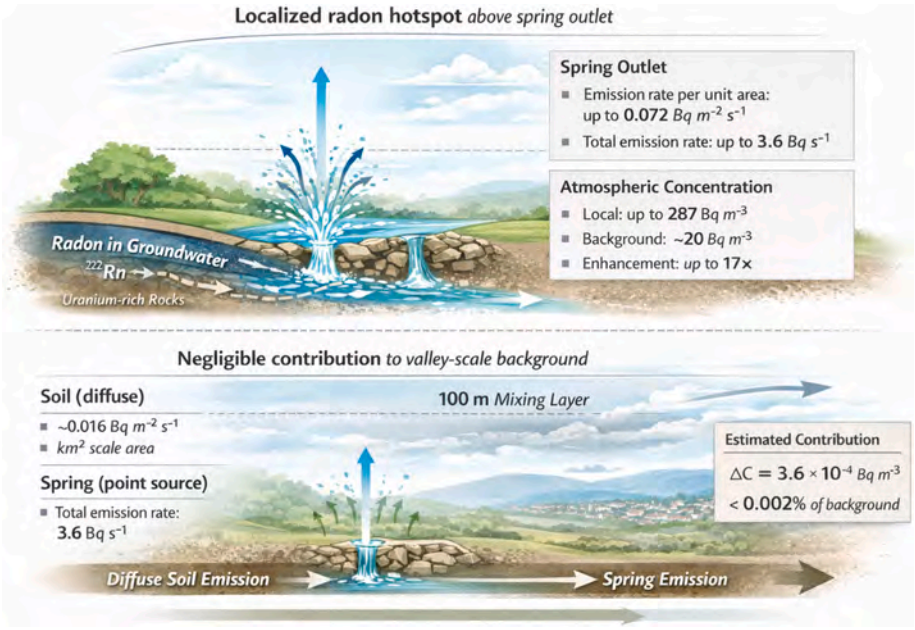

Fig. 8. Conceptual summary of radon emissions from groundwater-fed spring outlets and their atmospheric relevance across spatial scales.

conditions. Third, while the chamber-based accumulation method is widely used and suitable for localized flux quantification, uncertainties may arise from assumptions regarding effective degassing area, chamber positioning, and linear accumulation intervals. Finally, the order-of-magnitude atmospheric dilution estimate is based on simplified steady-state assumptions and does not account for complex three-dimensional dispersion processes; it is therefore intended as a conservative first-order approximation rather than a predictive dispersion model. The uncertainties associated with the chamber-based method are mainly systematic and consistently affect all measurements. Consequently, although they might alter the absolute values of the estimated emission rates, they do not affect relative comparisons between sites or seasons, ensuring the robustness of the statistical analysis.

Despite these limitations, the integrated observational design adopted here provides a coherent framework for distinguishing between high-intensity localized radon hotspots and negligible valley-scale atmospheric contributions. This approach may be applicable to other groundwater-fed systems in tectonically active carbonate aquifer environments influenced by major fault structures, where discrete degassing points coexist with diffuse soil emissions.

4. Conclusions

This study provides a quantitative multi-scale assessment of groundwater-derived radon emissions in a fault-influenced carbonate aquifer system by integrating direct emission rate measurements with year-long atmospheric monitoring. Field observations demonstrate that spring outlets can generate pronounced localized atmospheric radon enhancements, with concentrations up to 17 times background levels and emission rates per unit area reaching 0.072 Bq m^{-2} s^{-1}. These findings confirm that groundwater-fed springs may act as discrete outdoor radon hotspots under open-air conditions.

Despite their high local intensity, the integrated source strength of individual spring outlets remains limited when evaluated at the urban scale. Order-of-magnitude dilution estimates indicate that the maximum theoretical concentration increment attributable to a single spring ($<3.6 \times 10^{-4}$ Bq m^{-3}) represents less than 0.002% of the regional atmospheric background. Diffuse soil exhalation, therefore, remains the dominant contributor to valley-scale atmospheric radon levels.

Background monitoring revealed persistent diurnal cycles driven by boundary-layer dynamics, with morning concentrations averaging 2.3 times the afternoon minimum and a clear seasonal maximum in autumn. Meteorological controls were statistically significant but individually weak, whereas proxies of atmospheric stability (PM_{10}) explained a substantially larger fraction of radon variability, highlighting the dominant role of mixing-layer processes.

Overall, the results clarify the coexistence of high-intensity localized degassing and negligible regional-scale contribution within groundwater-dominated systems. By explicitly quantifying both emission fluxes and atmospheric response across spatial scales, this study refines the understanding of radon source apportionment in carbonate aquifer systems influenced by major fault structures and tectonic activity. Incorporating discrete groundwater-fed emission points into regional radon assessment frameworks may improve the representation of spatial heterogeneity in outdoor radon distributions, particularly in carbonate terrains where fault-controlled groundwater circulation enhances radon transport.

Funding

This research received no specific grant from any funding agency in the public, commercial, or not-for-profit sectors.

CRediT authorship contribution statement

Sumeya B. Abdella: Data curation, Investigation, Software, Visualization, Writing – original draft. **Michael T. Solomon:** Data curation, Formal analysis, Investigation, Visualization. **Luca Stabile:** Formal analysis, Resources, Supervision, Writing – review & editing. **Michele Saroli:** Conceptualization, Methodology, Supervision, Validation. **Giorgio Buonanno:** Conceptualization, Funding acquisition, Methodology, Project administration, Writing – review & editing.

Declaration of competing interest

The authors declare that they have no known competing financial interests or personal relationships that could have appeared to influence the work reported in this paper.

Data availability

Data will be made available on request.

References

Adyasari, D., Dimova, N.T., Dulai, H., Gilfedder, B.S., Cartwright, I., McKenzie, T., Fuleky, P., 2023. Radon-222 as a groundwater discharge tracer to surface waters. Earth Sci. Rev. 238, 104321. https://doi.org/10.1016/j.earscirev.2023.104321.

Al-Zoughool, M., Krewski, D., 2009. Health effects of radon: a review of the literature. Int. J. Radiat. Biol. 85, 57–69. https://doi.org/10.1080/09553000802635054.

ARPA Lazio, 2009. La Qualità Dell'Aria Della Provincia Di Frosinone. Anni 2006 -2007 - 2008. Agenzia Regionale per la Protezione dell'Ambiente dell Lazio.

Arvela, H., Holmgren, O., Hänninen, P., 2015. Effect of soil moisture on seasonal variation in indoor radon concentration: modelling and measurements in 326 Finnish houses. Radiat Prot Dosimetry ncv182. https://doi.org/10.1093/rpd/ncv182.

(UNSCEAR), 2000. Sources and effects of ionizing radiation. 1: sources. In: Report of the United Nations Scientific Committee on the Effects of Atomic Radiation. United Nations, New York.

Baltrėnas, P., Grubliauskas, R., Danila, V., 2020. Seasonal variation of indoor radon concentration levels in different premises of a university building. Sustainability 12, 6174. https://doi.org/10.3390/su12156174.

Bewick, V., Cheek, L., Ball, J., 2004. Statistics review 10 further nonparametric methods. Crit. Care 8, 196. https://doi.org/10.1186/cc2857.

Bossew, P., Lettner, H., 2007. Investigations on indoor radon in Austria, part 1: seasonality of indoor radon concentration. J. Environ. Radioact. 98, 329–345. https://doi.org/10.1016/j.jenvrad.2007.06.006.

Caracci, E., Canale, L., Buonanno, G., Stabile, L., 2022. Effectiveness of eco-feedback in improving the indoor air quality in residential buildings: mitigation of the exposure to airborne particles. Build. Environ. 226, 109706. https://doi.org/10.1016/j.buildenv.2022.109706.

Caracci, E., Iannone, A., Carriera, F., Notardonato, I., Pili, S., Murru, A., Avino, P., Campagna, M., Buonanno, G., Stabile, L., 2024. Size-segregated content of heavy metals and polycyclic aromatic hydrocarbons in airborne particles emitted by indoor sources. Sci. Rep. 14. https://doi.org/10.1038/s41598-024-70978-3.

Caracci, E., Stabile, L., Buonanno, G., 2021. A simplified approach to evaluate the lung cancer risk related to airborne particles emitted by indoor sources. Build. Environ. 204. https://doi.org/10.1016/j.buildenv.2021.108143.

Cartwright, I., Hofmann, H., 2016. Using radon to understand parafluvial flows and the changing locations ofgroundwater inflows in the avon river, southeast Australia. Hydrol. Earth Syst. Sci. 20, 3581–3600. https://doi.org/10.5194/hess-20-3581-2016.

Chambers, S., Williams, A.G., Zahorowski, W., Griffiths, A., Crawford, J., 2011. Separating remote fetch and local mixing influences on vertical radon measurements in the lower atmosphere. Tellus B 63, 843. https://doi.org/10.1111/j.1600-0889.2011.00565.x.

Choudhury, T.R., Ferdous, J., Haque, MdM., Rahman, MdM., Quraishi, S.B., Rahman, M. S., 2022. Assessment of heavy metals and radionuclides in groundwater and associated human health risk appraisal in the vicinity of Rooppur nuclear power plant, Bangladesh. J. Contam. Hydrol. 251, 104072. https://doi.org/10.1016/j.jconhyd.2022.104072.

Cook, P.G., 2013. Estimating groundwater discharge to rivers from river chemistry surveys. Hydrol. Process. 27, 3694–3707. https://doi.org/10.1002/hyp.9493.

Darby, S., Hill, D., Auvinen, A., Barros-Dios, J.M., Baysson, H., Bochicchio, F., Deo, H., Falk, R., Forastiere, F., Hakama, M., Heid, I., Kreienbrock, L., Kreuzer, M., Lagarde, F., Mäkeläinen, I., Muirhead, C., Oberaigner, W., Pershagen, G., Ruano-Ravina, A., Ruosteenoja, E., Rosario, A.S., Tirmarche, M., Tomáscaron, ek, L., Whitley, E., Wichmann, H.-E., Doll, R., 2005. Radon in homes and risk of lung cancer: collaborative analysis of individual data from 13 European case-control studies. Br. Med. J. 330, 223. https://doi.org/10.1136/bmj.38308.477650.63.

Dołhańczuk-Śródka, A., Janecki, D., Gawdzik, A., 2025. Radionuclides as inorganic contaminants of the aquatic environment. Desalination Water Treat. 321, 100946. https://doi.org/10.1016/j.dwt.2024.100946.

Čeliković, I., Pantelić, G., Vukanac, I., Krneta Nikolić, J., Živanović, M., Cinelli, G., Gruber, V., Baumann, S., Quindos Poncela, L.S., Rabago, D., 2022. Outdoor radon as a tool to estimate radon priority areas—A literature overview. IJERPH 19, 662. https://doi.org/10.3390/ijerph19020662.

Ellins, K.K., Roman-Mas, A., Lee, R., 1990. Using 222Rn to examine groundwater/surface discharge interaction in the Rio Grande de Manati, Puerto Rico. J. Hydrol. 115, 319–341. https://doi.org/10.1016/0022-1694(90)90212-G.

EPA, 2016. A Citizen's Guide to Radon: the Guide to Protecting yourself and your Family from Radon.

Etiope, G., Martinelli, G., 2002. Migration of carrier and trace gases in the geosphere: an overview. Phys. Earth Planet. Inter. 129, 185–204. https://doi.org/10.1016/S0031-9201(01)00292-8.

European Commission, 2013. Directive 2013/59/EURATOM of the European Parliament and of the Council of 5 December 2013 Laying down Basic Safety Standards for Protection Against the Dangers Arising from Exposure to Ionizing Radiation.

Fagerland, M.W., Sandvik, L., 2009. The wilcoxon–mann–whitney test under scrutiny. Stat. Med. 28, 1487–1497. https://doi.org/10.1002/sim.3561.

Florou, H., Kehagia, K., Savidou, A., Trabidou, G., 2006. The radiological evaluation of uranium, radium and radon in metallic and thermo-metallic springs in Ikaria Island, the eastern Aegean Sea, Greece. In: Radioactivity in the Environment. Elsevier, pp. 235–242. https://doi.org/10.1016/S1569-4860(05)08017-4.

Garzillo, C., Pugliese, M., Loffredo, F., Quarto, M., 2017. Indoor radon exposure and lung cancer risk: a meta-analysis of case-control studies. Transl. Cancer Res. 6, S934–S943. https://doi.org/10.21037/tcr.2017.05.42.

Gaskin, J., Coyle, D., Whyte, J., Krewksi, D., 2018. Global estimate of lung cancer mortality attributable to residential Radon. Environ. Health Perspect. 126, 057009. https://doi.org/10.1289/EHP2503.

GB 50325, 2020. GB 50325-2020: Standard for Indoor Environmental Pollution Control of Civil Building Engineering.

Guida, D., Guida, M., Lettieri, M., Tirri, V., Capacchione, B., 2014. Assessing radon-in-air from streamflow, comparing two study cases: Labso-Laura and Capodifiume springs (Campania region, southern Italy). https://doi.org/10.13140/2.1.4701.5046.

Hayashi, K., Yasuoka, Y., Nagahama, H., Muto, J., Ishikawa, T., Omori, Y., Suzuki, T., Homma, Y., Mukai, T., 2015. Normal seasonal variations for atmospheric radon concentration: a sinusoidal model. J. Environ. Radioact. 139, 149–153. https://doi.org/10.1016/j.jenvrad.2014.10.007.

Hoehn, E., Von Gunten, H.R., 1989. Radon in groundwater: a tool to assess infiltration from surface waters to aquifers. Water Resour. Res. 25, 1795–1803. https://doi.org/10.1029/WR025i008p01795.

Horváth, Á., Bohus, L.O., Urbani, F., Marx, G., Piróth, A., Greaves, E.D., 2000. Radon concentrations in hot spring waters in northern Venezuela. J. Environ. Radioact. 47, 127–133. https://doi.org/10.1016/S0265-931X(99)00032-6.

Iwata, D., Nagahama, H., Muto, J., Yasuoka, Y., 2018. Non-parametric detection of atmospheric radon concentration anomalies related to earthquakes. Sci. Rep. 8, 13028. https://doi.org/10.1038/s41598-018-31341-5.

Kolarž, P.M., Filipović, D.M., Marinković, B.P., 2009. Daily variations of indoor air-ion and radon concentrations. Appl. Radiat. Isot. 67, 2062–2067. https://doi.org/10.1016/j.apradiso.2009.07.023.

Koschorreck, M., Knorr, K.H., Teichert, L., 2022. Temporal patterns and drivers of CO2 emission from dry sediments in a groyne field of a large river. Biogeosciences 19, 5221–5236. https://doi.org/10.5194/bg-19-5221-2022.

Manawi, Y., Hassan, A., Atieh, M.A., Lawler, J., 2024. Overview of radon gas in groundwater around the world: health effects and treatment technologies. J. Environ. Manag. 368, 122176. https://doi.org/10.1016/j.jenvman.2024.122176.

Mullinger, N.J., Binley, A.M., Pates, J.M., Crook, N.P., 2007. Radon in Chalk streams: spatial and temporal variation of groundwater sources in the Pang and Lambourn catchments, UK. J. Hydrol. 339, 172–182. https://doi.org/10.1016/j.jhydrol.2007.03.010.

Nayak, T., Basak, S., Deb, A., Dhal, P.K., 2022. A systematic review on groundwater radon distribution with human health consequences and probable mitigation strategy. J. Environ. Radioact. 247, 106852. https://doi.org/10.1016/j.jenvrad.2022.106852.

Ongori, J.N., Lindsay, R., Mvelase, M.J., 2015. Radon transfer velocity at the water–air interface. Appl. Radiat. Isot. 105, 144–149. https://doi.org/10.1016/j.apradiso.2015.07.058.

Piersanti, A., Cannelli, V., Galli, G., Soldati, G., Piochi, M., Iovine, R.S., Pignatelli, A., Vignoli, V., Romoli, G., Albano, M., Antonioli, A., Ciaccio, M.G., D'Alessandro, A., De Astis, G., Farroni, S., Figlioli, A., Giunchi, C., Massa, M., Moro, M., Nardi, A., Saroli, M., Silvestri, M., Scudero, S., Vallocchia, M., 2025. Soil Radon time series from the Italian Radon Monitoring Network (IRON). Sci. Data 12, 415. https://doi.org/10.1038/s41597-025-04735-0.

Pignatelli, A., Romoli, G., Vignoli, V., 2025. A study of the radon seasonality with temporal dummy variables. Sci. Rep. 15, 30154. https://doi.org/10.1038/s41598-025-15710-5.

Podstawczyńska, A., Kozak, K., Pawlak, W., Mazur, J., 2010. Seasonal and diurnal variation of outdoor radon (222Rn) concentrations in urban and rural area with reference to meteorological conditions. Nukleonika 55, 543–547.

Pyuskyulyan, K., Pipoyan, D., Hovhannisyan, S., Beglaryan, M., Movsisyan, N., Belyaeva, O., 2024. Assessing radon hazard in drinking water: a comprehensive approach integrating deterministic and probabilistic methods with water consumption routines. Sci. Total Environ. 949, 175217. https://doi.org/10.1016/j.scitotenv.2024.175217.

Rathebe, P.C., Mphaga, K.V., Masekameni, D.M., 2025. Climate change and environmental radioactivity: a review of studies on climate conditions in variation on indoor radon concentrations. Environ. Monit. Assess. 197, 446. https://doi.org/10.1007/s10661-025-13889-8.

Repubblica Italiana, 2020. Official Journal [WWW Document]. URL. https://www.gazzettaufficiale.it/eli/id/2020/08/12/20G00121/sg, 2.16.26.

Saroli, M., Albano, M., Modoni, G., Moro, M., Milana, G., Spacagna, R.-L., Falcucci, E., Gori, S., Scarascia Mugnozza, G., 2020. Insights into bedrock paleomorphology and linear dynamic soil properties of the Cassino intermontane basin (Central Italy). Eng. Geol. 264, 105333. https://doi.org/10.1016/j.enggeo.2019.105333.

Saroli, M., Lancia, M., Albano, M., Modoni, G., Moro, M., Scarascia Mugnozza, G., 2014. New geological data on the Cassino intermontane basin, central Apennines, Italy. Rend. Fis. Acc. Lincei 25, 189–196. https://doi.org/10.1007/s12210-014-0338-5.

Saroli, M., Lancia, M., Petitta, M., 2019. The geology and hydrogeology of the Cassino plain (central Apennines, Italy): redefining the regional groundwater balance. Hydrogeol. J. 27, 1563–1579. https://doi.org/10.1007/s10040-019-01953-w.

Schubert, M., Musolff, A., Weiss, H., 2018. Influences of meteorological parameters on indoor radon concentrations (222Rn) excluding the effects of forced ventilation and radon exhalation from soil and building materials. J. Environ. Radioact. 192, 81–85. https://doi.org/10.1016/j.jenvrad.2018.06.011.

Sola, P., Srisuksawad, K., Loaharojanaphand, S., O-Manee, A., Permnamtip, V., Issarapan, P., Thummagarun, L., 2012. Radon concentration in air, hot spring water,

and bottled mineral water in one hot spring area in Thailand. J. Radioanal. Nucl. Chem. 297. https://doi.org/10.1007/s10967-012-2359-9.

Sulaiman, M.B., Lawal, R.S., Yusuf, A., Abubakar, A., Rafi, A.B., 2025. Evaluation of radon in surface water and groundwater around an illegal mining site in Dareta, Zamafara, Nigeria: assessing potential health risks. J. Radioanal. Nucl. Chem. 334, 1613–1620. https://doi.org/10.1007/s10967-024-09941-5.

Sun, X., Du, Y., Tian, H., Xu, J., Shi, H., Liu, Y., Deng, Y., Gan, Y., Wang, Y., 2025. Seasonal dynamics of closed lakes nutrient status controlled by lacustrine groundwater discharge. EGUsphere 2025, 1–21. https://doi.org/10.5194/egusphere-2025-5433.

Tallini, M., Guerriero, V., Nyberg, A.A., Wyss, R., Barberio, M.D., Carafa, M.M.C., De Luca, G., Di Naccio, D., Frepoli, A., Kastelic, V., Pizzino, L., Saroli, M., Sciortino, A., Scorzini, A.R., Gerl, J., Kumar, G., Bäck, T., Karakostas, V., Kourouklas, C., Papadimitriou, E., Stoulos, S., 2025. Selection of hydrosensitive to seismicity sites for radon monitoring in the Abruzzo aquifers (central Italy) within the European ArtEmis project. Phys. Chem. Earth, Parts A/B/C 141, 104127. https://doi.org/10.1016/j.pce.2025.104127.

UNSCEAR, 2000. United Nations Scientific Committee on the Effects of Atomic Radiation. Sources and Effects of Ionizing Radiation. United Nations Scientific Committee on the Effects of Atomic Radiation. New York.

Vienneau, D., Boz, S., Forlin, L., Flückiger, B., De Hoogh, K., Berlin, C., Bochud, M., Bulliard, J.-L., Zwahlen, M., Röösli, M., 2021. Residential radon – comparative analysis of exposure models in Switzerland. Environ. Pollut. 271, 116356. https://doi.org/10.1016/j.envpol.2020.116356.

Walczak, K., Olszewski, J., Zmyślony, M., 2016. Radon permeability of insulating building materials. Nukleonika 61, 289–293. https://doi.org/10.1515/nuka-2016-0048.

Yarmoshenko, I., Malinovsky, G., Vasilyev, A., Onishchenko, A., 2021. Model of radon entry and accumulation in multi-flat energy-efficient buildings. J. Environ. Chem. Eng. 9, 105444. https://doi.org/10.1016/j.jece.2021.105444.

Zahorowski, W., Chambers, S.D., Henderson-Sellers, A., 2004. Ground based radon-222 observations and their application to atmospheric studies. J. Environ. Radioact. 76, 3–33. https://doi.org/10.1016/j.jenvrad.2004.03.033.

Zeeb, H., Shannoun, F., World Health Organization, 2009. WHO Handbook on Indoor Radon: a Public Health Perspective.